Supramolecular Assembly between Cationic Pyridinium-Pillararene and Aminosalicylate Drug

Willian Demos,[a] Lizandra C. B. Micke,[a] Luis H. S. Lacerda,[b] Bruno S. Souza,[a] Adriana P. Gerola [,a] and Ricardo F. Affeldt [*,a]*

[a]*Laboratório de Catálise e Fenômenos Interfaciais, Departamento de Química, Universidade Federal de Santa Catarina, 88040-900 Florianópolis-SC, Brazil*

[b]*Grupo de Estrutura Eletrônica Molecular, Departamento de Química, Universidade Federal de Santa Catarina, 88040-900 Florianópolis-SC, Brazil*

The preparation and characterization of a novel pillar[5]arene based supramolecular system with mesalazine, a prescribed aminosalicylate drug was successfully achieved. Pyridinium-pillar[5]arene was efficiently prepared in three steps from hydroquinone bis(2-hydroxyethyl) ether derivative in high yield. It was demonstrated that the association between the compounds is pH dependent with an association constant of 3.4×10^3 L mol^{-1} near physiological conditions, leading to quenching of the fluorescence emission of mesalazine in the presence of the cationic macrocycle. Theoretical calculations indicate that the association between both molecules is of electrostatic nature. Formation of aggregates was also demonstrated in low concentrations of pillar[5]arene that is related to the non-linear behavior of the Stern-Volmer plot for quenching of mesalazine fluorescence emission.

Keywords: supramolecular, mesalazine, pillararene, fluorescence, DFT

Introduction

Since its first report in 2008, pillararenes[1] have been the goal of many studies in different fields being applied as chemosensors,[2] drug delivery systems[3] and as supramolecular catalysts and nanoreactors based on the host-guest properties.[4] Pillararenes are prepared by condensation of hydroquinone with paraformaldehyde leading to a methylene bridged symmetric structure with a rich electron π-cavity which allows complexation with small molecules in a system that resemble the enzyme receptor-ligand complex.[5-7] Although the described features, the groups in the so-called portals of pillararenes are of extreme relevance in induction and pre-complexation of the ligand and those are of easy functionalization by neutral or charged groups from nucleophilic displacement of leaving groups (Figure 1), being responsible for increasing intermolecular interactions with the guest molecules.[8]
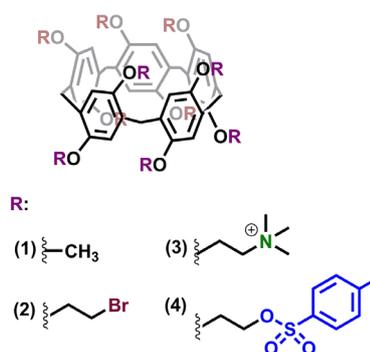

Figure 1. Structure of pillar[5]arene and its versatility with neutral or charged groups from substitution reactions.

The influence of these groups associated with aryl cavity size was explored in important applications such as recognition of environmental contaminants[9,10] or even in the eradication of diseases.[11] Also, the formation of supramolecular complexes based on the nature of the interactions with the hydrophobic cavity and both functionalized portals allow great association with other compounds and may be modulated to mimic natural processes and to develop smart drug delivery systems to biologically active compounds.[10,12-15] The non-covalent interactions between the macrocycle and a ligand can

*e-mail: ricardo.affeldt@ufsc.br; adriana.gerola@ufsc.br
Editor handled this article: Paula Homem-de-Mello (Associate)

modify properties such as solubility, stability and optical properties, among others.[16-19]

In the past few years, we dedicated our efforts to prepare supramolecular systems from differently functionalized pillararenes for molecular recognition of drugs such as methamphetamine and for creating an appropriate environment for degrading highly toxic compounds such as model pesticides phosphates.[20,21] Other publication[22] from our research group showed that it was possible to tune reactivity of guest molecules based on the pillararene structure. It is also important to mention that good compatibility with human organism with low cytotoxicity was already evidenced for pillararenes which increase the range of application of these compounds for medical purposes.[15] Cationic pillararenes, for instance, have been described as successful inhibitors of biofilm growth by Gram-positive bacteria, which are strictly related to antibiotic resistance[23,24] Also, these compounds can form supramolecular complex systems with other nanomaterials envisioning guest delivery for medical uses that are typically pH-responsive.[25]

On the other hand, inflammatory bowel diseases (IBD) have increased being Chron's disease and ulcerative colitis the most frequent in the western population.[26-28] These diseases do not present a cure; however, treatment provides the patient a good quality of life. Currently, the most prescribed drug for IBD treatment is mesalazine (MSZ), also known as 5-aminosalicylic acid which acts directly on the inhibition of enzymes such as cyclooxygenase and lipoxygenase, also inhibiting the death of active cells. Considering the importance of this class of aminosalicylate anti-inflammatory drugs, different detection and delivery systems have been studied to increase solubility in aqueous media and permeability in membranes.[29-31] Thus, in this work, we synthesized a cationic pyridinium-pillar[5]arene (P[5]Py) and investigated the formation of supramolecular mesalazine pillar[5]arene complexes by fluorescence spectroscopy, nuclear magnetic resonance (NMR), and theoretical calculations. Supramolecular complexation led to quenching of fluorescence, which was evaluated by quenching models and fluorescence lifetime. The high association and quenching constant values of mesalazine and pillar[5]arene are interesting results for future work on release and quantification systems for mesalazine.

Experimental

Materials and methods

Chemicals

All materials were purchased from Sigma-Aldrich (Darmstadt, Germany) and used as received. Acetonitrile and dichloroethane were dried over 4 Å molecular sieves. Pyridine was not previously distilled.

NMR spectra

The NMR spectra were made using Bruker AC 200 and 400 MHz spectrometers. ^{1}H NMR spectra were recorded either at 200 or 400 MHz and ^{13}C NMR at 50 or 101 MHz, respectively with tetramethylsilane (TMS or TMSP) as internal standard (0.00 ppm) in CDCl$_3$ or D$_2$O. Nuclear Overhauser effect (NOESY) correlation spectra (mixing time = 1.0 s) were conducted for supramolecule in D$_2$O in adjusted pHs = 1.0, 5.0 and 7.5 (pD = pH + 0.44). NMR spectra were processed using TopSpin 1.3 and MestReNova 7.0.

FTIR spectra

The IR spectra were recorded using ABB FTLA 2000 spectrometer (Zurich, Switzerland) with KBr dispersed solid samples. No significant changes were observed for the mixture of MSZ and P[5]Py compared to the pure compounds. The Fourier transform infrared spectroscopy (FTIR) data obtained were processed using Origin 8.0.[32]

HRMS measurements

High-resolution mass spectrometry (HRMS) analysis was performed using the turbo ion spray source (electrospray ionization-ESI), Applied Biosystems/MDS Sciex (Concord, Canada) in positive ion mode. Samples were infused continuously at 10 μL min^{-1} with a syringe pump. The capillary needle voltage was maintained at 4.5 kV. The mass spectrometry (MS/MS) parameters were curtain gas, 10 psi; ion spray interface, 0.0 °C; GS1, 18.0 psi; GS2, 0.0 psi; and collision gas, medium.

UV-Vis measurements

All the UV-Vis measurements were made in aqueous media with a spectrophotometer Cary 50 from Varian (Shelton, USA) equipped with a thermostatic bath using quartz cuvettes, with 1.0 cm of the optical path. The pH of the measurements were maintained using buffers solutions (0.01 mol L^{-1}): chloroacetic acid (pK_a 2.8), sodium acetate (pK_a 4.6), Bis-Tris (pK_a 6.5) and Tris (pK_a 8.25). To P[5]Py the absorption was followed at 291 nm and to MSZ the absorption was followed in 298 and 330 nm. The absorbance data obtained were processed using Origin 8.0.[32]

Fluorescence measurements

The fluorescence measurements were made with a spectrofluorimeter Cary Eclipse from Varian (Melbourne, Australia), with a xenon lamp of 450 W as excitation font, with variables slits and adjustable voltages. To

mesalazine (MSZ) measurements, the fluorescence spectra were obtained with excitation at 298 or 330 nm, with a slit of 5 nm. Titration experiments were conducted by monitoring MSZ fluorescence emission maxima (500 nm) at pH 7.5 increasing the concentration of P[5]Py on a solution or MSZ from 2.9×10^{-5} to 3.2×10^{-4} mol L^{-1} (excess of 20 equivalents of P[5]Py). The fluorescence data obtained were processed using Origin 8.0.[32] To obtain the association constant (K) value for MSZ $\subset$ P[5]Py system, the equation 1 was used:

$$I = \frac{I_0 + IK[M][P]}{1 + K[P]} \tag{1}$$

where I_0 and I are the fluorescence intensity of MSZ in the absence and presence of P[5]Py, respectively, [M] is the concentration of MSZ, [P] is the concentration of P[5]Py.

The fluorescence quantum yield (Φ_f) of MSZ at different pH was calculated using equation 2, and the MSZ at pH 4 as a standard ($\Phi_{std} = 0.06$).[33]

$$\Phi_f = \frac{A_{std} \times F_{MSZ} \times n_{std}^2 \times \Phi_{std}}{A_{MSZ} \times F_{std} \times n_{MSZ}^2} \tag{2}$$

where A_{std} and F_{std} are the absorbance and fluorescence of MSZ in pH 4, used as a standard for the calculations. A_{MSZ} and F_{MSZ} are the absorbance and fluorescence in different pH's. The both terms n_{std}^2 and n_{MSZ}^2 refer to refractive index of water.

Fluorescence lifetime measurements

All fluorescence lifetime experiments were performed using a spectrofluorimeter Easy Life V, Optical Building Blocks Corporation (Birmingham, England). For each analysis, a light emitting diode (LED) with a wavelength of 370 nm was used, with a filter of 10 nm bigger than LED wavelength. The IRF used was LUDOX® 30% in aqueous media. The quality of the fitting (exponential decay) was monitored by chi-squared values. The fluorescence lifetime measurements data obtained were processed using Origin 8.0.[32]

Conductivity measurements

Conductivity measurements were performed using a Metrolhm Model 712 conductivity meter (Herisau, Switzerland), using a thermostatic cell at 25 °C, with an initial volume of 20 mL of a buffered aqueous solution, at pH = 7.5. The titrations were performed to evaluate the P[5]Py self-assembly. The conductivity data obtained were processed using Origin 8.0.[32]

DLS

Hydrodynamic diameters of the aggregates were determined using dynamic light scattering (DLS) equipment-Malvern Instruments Zetasizer Nano Series (Worcestershire, England). The measurements were used to evaluate the average size of P[5]Py aggregates. The concentration of P[5]Py = 1.2×10^{-4} mol L^{-1} was used for the experiment. All measurements were performed at pH = 7.5, at 25 °C. The DLS data obtained were processed using Zetasizer Software 7.12.

Synthesis

Bromination of hydroquinone bis(2-hydroxyethyl) ether (HQBr, compound **2**)[1,34]

In a reaction flask, under an argon atmosphere, hydroquinone bis(2-hydroxyethyl) ether (**1**, 10.0 mmol) and triphenyl phosphine were dissolved in CH$_3$CN (50 mL) and the mixture was cooled to 0 °C. Then, tetrabromomethane (23.8 mmol) was slowly added and the reaction mixture was stirred for 4 h at room temperature. After this time, cold water was added to afford a white precipitate, which was further filtrated and washed with cold MeOH to afford product **2** as a white crystal. Yield 75%; ^{1}H NMR (200 MHz, CDCl$_3$) δ 6.86 (s, 4H), 4.25 (t, *J* 6.3 Hz, 4H), 3.62 (t, *J* 6.3 Hz, 4H); ^{13}C NMR (50 MHz, CDCl$_3$) δ 152.5, 116.3, 68.9, 29.4.

Tosylation of hydroquinone bis(2-hydroxyethyl) ether (HQOTs, compound **3**)[7]

In a reaction flask, an aqueous solution of NaOH (70 mmol, 4 mL) was added to a solution of, hydroquinone bis(2-hydroxyethyl) ether (1, 11.6 mmol), in tetrahydrofuran (THF, 20 mL), and the mixture was cooled to 0 °C. Then, under stirring, 4-methylbenzenesulfonyl chloride (26.2 mmol) was dropwisely added and the system was stirred for 2 h at room temperature. After this time, the reaction was poured into ice-cold water and the product was extracted with CH$_2$Cl$_2$. The organic phase was washed with water, brine and dried with MgSO$_4$. Product **3** was further obtained after solvent removal to afford a white powder. Yield 65%; ^{1}H NMR (400 MHz, CDCl$_3$) δ 7.82, 7.35, 6.69, 4.34, 4.33, 4.32, 4.10, 4.08, 4.07, 2.45; ^{13}C NMR (50 MHz, CDCl$_3$) δ 151.9, 150,0, 147.5, 131.8, 130.9, 118.6, 69.9, 63.6, 32.1.

Synthesis of tosylated pillar[5]arene (P[5]OTs, compound **4**)[7]

A solution of paraformaldehyde (8.97 mmol) and boron trifluoride diethyl etherate (3.06 mmol) in dry dichloroethane (25 mL) was stirred for 10 min. Then, a solution of tosylated hydroquinone bis(2-hydroxyethyl)

J. Braz. Chem. Soc. **2024**, *35*, 1, e-20230106

3 of 11

ether (**3**, 10.3 mmol) in dry dichloroethane (25 mL) was added dropwisely and the reaction was stirred for 4 h under argon atmosphere. After this time, the mixture was diluted in methanol (50 mL) and dichloromethane (150 mL) and the mixture was washed with water (3 × 50 mL) and brine. The organic layer was dried over $MgSO_4$ and the solvent was removed under reduced pressure. Product **4** was purified by flash column chromatography 99:1, CH_2Cl_2:MeOH resulting in P[5]OTs as a white solid. Yield 31%; ^{1}H NMR (200 MHz, $CDCl_3$) δ 7.71 (d, *J* 8.3 Hz, 20H), 7.04 (d, *J* 8.0 Hz, 20H), 6.78 (s, 10H), 4.54-4.40 (m, 10H), 4.39-4.31 (m, 10H), 4.29-4.17 (m, 10H), 4.15-3.95 (m, 10H), 3.60 (s, 10H), 2.27 (s, 30H); ^{13}C NMR (50 MHz, $CDCl_3$) δ 149.5, 145.0, 132.2, 129.8, 128.4, 127.7, 114.41, 69.6, 65.7, 31.1, 21.6.

Synthesis of brominated pillar[5]arene (P[5]Br, compound **5**)[1,34]

To a solution of brominated hydroquinone bis(2-hydroxyethyl) ether (**2**, 10.3 mmol) in dry dichloroethane and argon atmosphere, paraformaldehyde (30.9 mmol) was added, and the system stirred for 30 min. After this time, boron trifluoride diethyl etherate (10.9 mmol) was slowly added to the system and the mixture was stirred at room temperature for 2 h. After this time, the mixture was washed with water, brine and sodium bicarbonate. The organic layer was dried over $MgSO_4$ and the solvent was removed under reduced pressure. Product **5** was purified by flash column chromatography 1:1, CH_2Cl_2:hexane resulting in P[5]Br as a white solid. Yield 65%; ^{1}H NMR (200 MHz, $CDCl_3$) δ 6.91 (s, 10H), 4.23 (t, *J* 5.5 Hz, 20H), 3.84 (s, 10H), 3.63 (t, *J* 5.4 Hz, 20H); ^{13}C NMR (50 MHz, $CDCl_3$) δ 149.9, 129.3, 116.3, 69.1, 30.8, 29.5.

Synthesis of pyridinium-pillar[5]arene (P[5]Py, compound **7**) from P[5]Br[24]

In a reaction flask P[5]Br (**5**, 0.5 mmol) and 10 mL of pyridine were stirred for 48 h at 80 °C. After this time, the excess of pyridine was removed by vacuum and the remaining solid was washed with ethyl ether until the solvent comes out colorless. Then, the crude product was washed with ethanol and precipitated in ethyl ether forming a fine precipitate that could be removed by centrifugation. The product P[5]Py **7** was obtained as a flavescent powder. Yield 96%; ^{1}H NMR (200 MHz, D_2O) δ 8.70 (d, *J* 5.5 Hz, 20H), 8.30 (t, *J* 8.0 Hz, 10H), 7.88 (d, 20H), 6.53 (s, 10H), 4.92 (t, 20H), 4.46 (t, 20H), 3.39 (s, 10H); ^{13}C NMR (50 MHz, D_2O) δ 152.1, 149.1, 147.6, 131.9, 131.0, 118.7, 70.1, 63.8, 32.2; HRMS *m/z*, calcd. for $[C_{105}H_{109}N_{10}O_{10}]$ 10+: 1669.8378, found: 1670.2191.

Synthesis of pyridinium pillar[5]arene (P[5]Py, compound **6**) from P[5]OTs[7]

In a reaction flask P[5]OTs (**4**, 0.5 mmol) and 10 mL of pyridine were stirred for 48 h at 80 °C. After this time, the excess of pyridine was removed under vacuum and the remaining solid was washed with ethyl ether until the solvent comes out colorless. Then, the crude product was washed with ethanol and precipitated in ethyl ether forming a fine precipitate that could be removed by centrifugation. The product P[5]Py was obtained as a flavescent powder. Yield 50%; ^{1}H NMR (200 MHz, D_2O) δ 8.90 (d, *J* 5.6 Hz, 20H), 8.56 (t, *J* 8.0 Hz, 10H), 8.06 (d, *J* 7.0 Hz, 20H), 7.56 (d, *J* 8.0 Hz, 20H), 6.91 (d, *J* 8.2 Hz, 20H), 6.62 (s, 10H), 5.01 (s, 20H), 4.32 (s, 20H), 3.38 (s, 10H), 1.79 (s, 30H); ^{13}C NMR (101 MHz, D_2O) δ 148.9, 146.3, 144.6, 141.8, 139.8, 129.2, 129.0, 128.3, 125.0, 115.7, 67.4 (s), 60.7, 20.0.
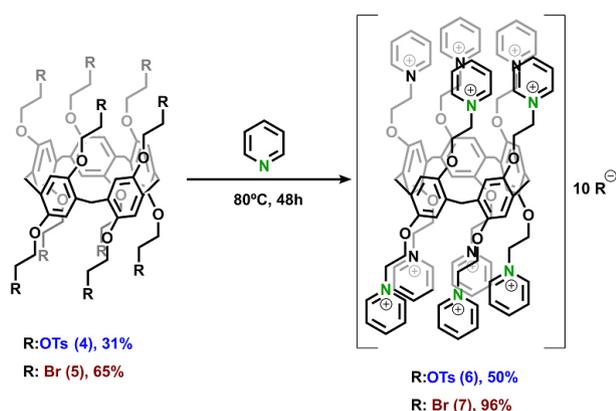
Computational details

The MSZ and P[5]Py structures obtained were previously optimized using semi-empirical xTB(extended Tight Binding)[35] developed by Stefan Grimme.[36] The xTB package was employed to minimize the computational cost to obtain more accurate theoretical results. The obtained structures are then fully optimized using density functional theory (DFT)[37] allied to BP86 Generalized Gradient Approximation (GGA) functional to description of Exchange correlation terms and D3 Grimme corrections.[38] The atoms were described by valence triplezeta basis set with updated polarization functions (def2-TZVP). Frequency calculations were carried out to guarantee that a minimum structure was obtained, as evidenced by the absence of imaginary eigenvalues in the Hessian matrix. The MSZ and P5Py structures obtained from DFT calculations were combined to evaluate the interaction between both molecules; the combined models were also optimized using xTB and DFT/BP86 calculations. TDDFT calculations employing B3LYP hybrid functional were also performed to predict UV-Vis spectra for MSZ on water solvent; the theory level was increased for such calculation to describe excited states more precisely. All calculations performed in this work employ the Orca quantum code.[39]

Results and Discussion

Synthesis

Synthesis of the pyridinium-pillar[5]arene (P[5]Py, compound **7**) was performed starting from brominated pillararene according to Scheme 1. Analysis of ^{1}H NMR,

^{13}C NMR and ESI-MS have confirmed the obtention of the cationic macrocycle as bromide salt. ^{1}H NMR spectra show well-defined signals that are in agreement with the proposed structure by Cohen and co-workers.[24] Also, we have prepared a tosylate salt of pyridinium-pillar[5] arene (compound **6**) using a different strategy than the one proposed by Ogoshi,[1,5] avoiding the use of carbon tetrabromide and triphenylphosphine. Nevertheless, it is interesting to observe that the methylene bridged hydrogens of P[5]Py are highly shielded compared to other pillararene structures (3.39 ppm compared to 3.84 ppm for P[5]Br, see Supplementary Information (SI) section, Figures S4 and S10).

Scheme 1. Synthesis of pyridinium-pillar[5]arene by substitution of different leaving groups.

Characterization

Mesalazine was achieved from commercial source and was previously characterized concerning its optical properties. The pK_a values (Figure 2) were determined by spectrophotometric titration (calibration curves shown in the SI section, Figures S14-S16).[40,41] The distribution of the species in equilibria is also shown in Figure 2.
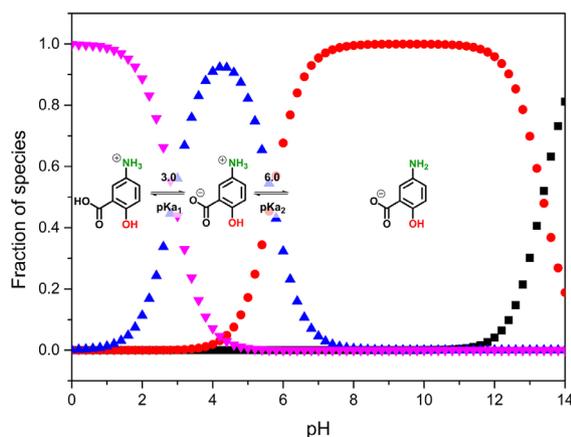

Figure 2. Distribution of MSZ species and molar fractions of MSZ as a function of pH. Graph obtained by CurTiPot.[42]

The influence of pH in UV-Vis absorption and fluorescence emission intensities of MSZ was analyzed as shown in Figure 3. In acidic pH, MSZ shows an absorption band at 298 nm ($\varepsilon = 3.7 \times 10^3$ L mol^{-1} cm^{-1}, see Table 1, π-π* transition) attributed to cationic compound **8**. Between pH 5.5-6.0 two bands from species **9** and **10** are present. However, above pH = 6.0, the maximum absorption suffers a bathochromic effect, 330 nm ($\varepsilon = 4.00$ L mol^{-1} cm^{-1}, see Table 1, π-π* transition) due to higher solvation of the anionic specie **10** (Figure 3). The fluorescence emission profile of MSZ is observed in Figure 4, with a dual fluorescence emission ($l_1 = 400$ nm and $l_2 = 500$ nm). A large Stokes shift (ca. 100×10^3 cm^{-1}) is observed for the lower energy band (Figure 4a, Table 1). This was expected since the excited state intramolecular proton transfer (ESIPT) is widely observed for salicylic acids derivatives and the emission bands are ascribed to normal (N*) and tautomeric (T*) excited states.[7,33,42-45] The pH has a major influence on the stabilization of the keto tautomer resulting in a single emission band at 500 nm for pH above 6.0 (Figure 4b), and in this case the Stokes shifts were at around 50×10^3 cm^{-1}. Complete photophysical data are summarized on Table 1. We have conducted the following experiments under physiological conditions, where the fluorescence intensity is notably high (Figure 4c), and high fluorescence quantum yield values are observed (Table 1).
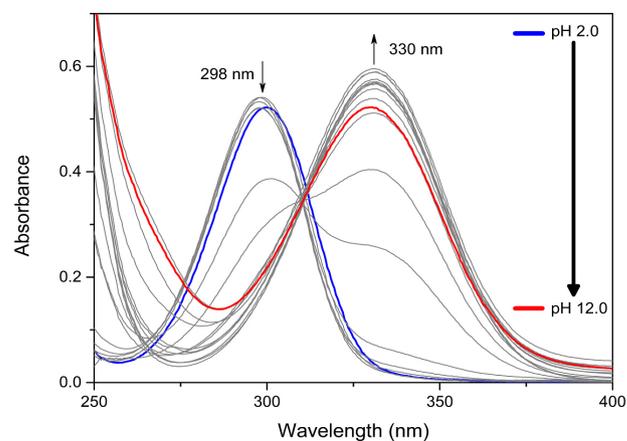

Figure 3. UV-Vis absorption spectra of MSZ in water (1.4×10^{-4} mol L^{-1}) at pH range 2.0-14.0, step = 0.5.

We started spectrofluorimetric titration experiments to investigate a possible complexation between P[5]Py and MSZ at pH 7.5 since MSZ is the sole fluorescence emitting specie, monitoring the band located at 500 nm. With successive addition of P[5]Py ranging from 0 to 20 equivalents it was possible to observe quenching of fluorescence emission of MSZ above 2.0×10^{-3} mol L^{-1} of P[5]Py (Figure 5). The area under the curves of fluorescence emission was chosen to not neglect any normal (N*)

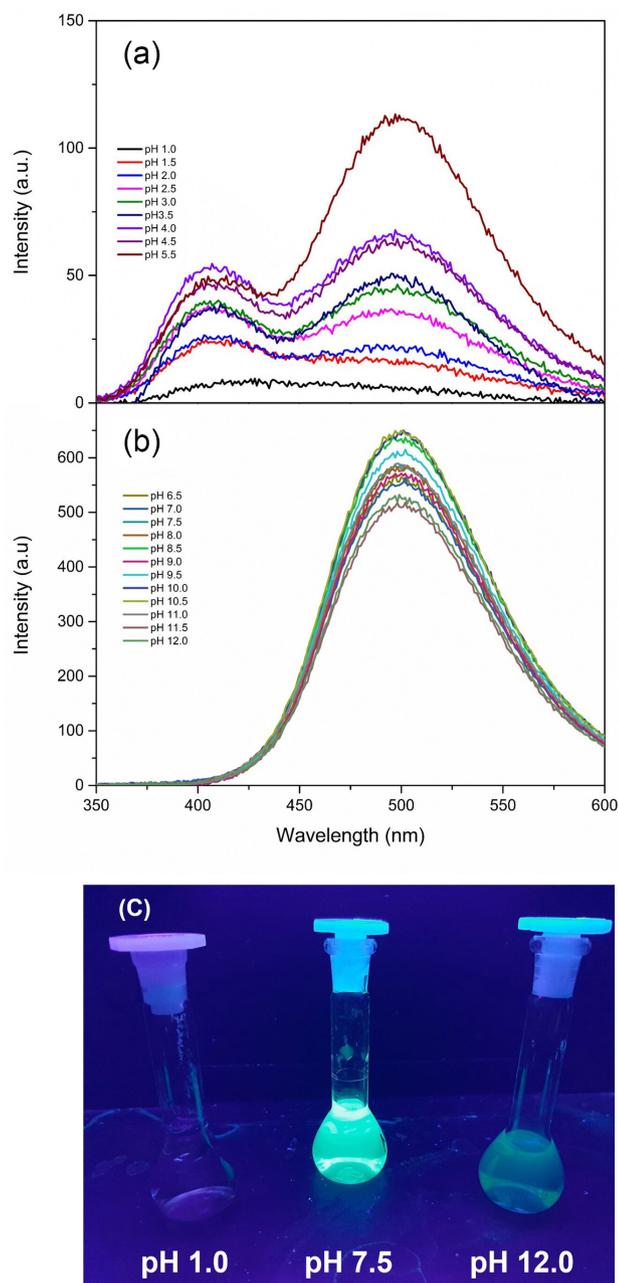**Figure 4.** (a) Fluorescence emission spectra of MSZ (1.4×10^{-4} mol L^{-1}) in water at pH 1-5.5 with λ_{exc} = 298 nm; (b) fluorescence emission spectra of MSZ (1.4×10^{-4} mol L^{-1}) in water at pH 6.5-12.0 with λ_{exc} = 330 nm; and (c) visual fluorescence emission of solutions irradiated at 365 nm.

Table 1. Photophysical data of MSZ, wavelength of maximum absorption (λ_{abs}) and emission (λ_{em}), Stokes shift ($\Delta\nu$), fluorescence quantum yield (Φ) and molar absorption coefficient (ε), as a pH function

pH	λ_{abs} / nm	λ_{em} / nm	$\Delta\nu$ / (10^3 cm^{-1})	Φ	ε^a / (10^3 L mol^{-1} cm^{-1})
2.0	299	500	99.0	0.024	3.71
2.5	298	500	98.0	0.035	3.85
3.0	297	500	97.1	0.043	3.71
3.5	297	500	97.1	0.038	3.84
4.0	297	500	97.1	0.060	3.81
4.5	298	500	98.0	0.057	3.71
5.5	300	500	100.0	0.12	2.71
6.5	330	500	50.8	0.34	3.65
7.0	330	500	50.8	0.32	4.00
7.5	330	500	50.8	0.33	4.00
8.0	330	500	50.8	0.32	4.07
8.5	330	500	50.8	0.35	4.07
9.0	330	500	50.8	0.31	4.00
9.5	330	500	50.8	0.33	4.19
10.0	330	500	50.8	0.35	4.24
10.5	330	500	50.8	0.34	4.17
11.0	330	500	50.8	0.33	4.07
11.5	330	500	50.8	0.30	3.86
12.0	330	500	50.8	0.32	3.73

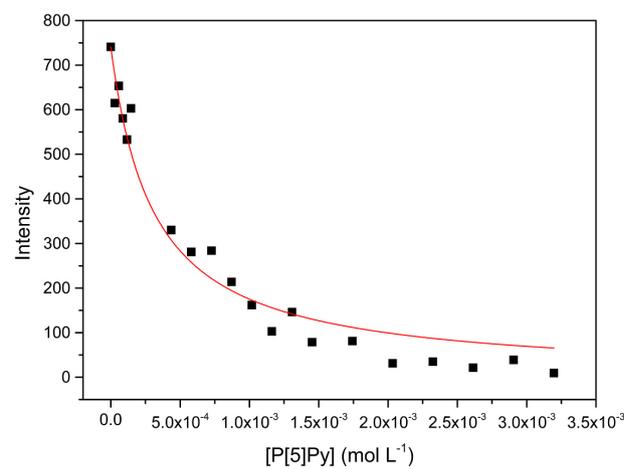$^a\varepsilon$ values were obtained at maximum absorption wavelengths (λ_{abs}).

Figure 5. Quenching on fluorescence emission of MSZ (1.4×10^{-4} mol L^{-1}) by successive additions of P[5]Py at pH 7.5.

emission band at 400 nm. Nevertheless, the plot *versus* fluorescence emission intensity showed essentially the same results. It is worth mentioning that the presence of P[5]Py stabilizes the ESIPT band at 500 nm for all pH values (see SI section, Figures S17-S19), suppressing the band for normal emission.

The formation of inclusion complexes of mesalazine with β-cyclodextrin (CD), hydroxypropyl-β-cyclodextrin (HP-β-CD) and 18-crown-6 ether (18C6) were already investigated.[30,31,46,47] These molecules present higher diameters of the hydrophobic cavity that are capable of hosting the aromatic extent of the MSZ molecule in a 1:1 stoichiometry. When the same models were applied to our system, they resulted in association constants that are up to 30-fold higher than the previous ones (Table 2). That suggests that the strong interaction between the compounds is related to charge interactions, increasing the tendency of complexation.

Table 2. Association constant (K) between MSZ and different macrocycles

Inclusion complex	K / (L mol^{-1})	Reference
MSZ⊂β-CD	1.36×10^2	Elbashir *et al.*[30]
MSZ⊂β-CD	6.96×10^2	Karpour *et al.*[46]
MSZ⊂18C6	1.41×10^2	Elbashir *et al.*[29]
MSZ⊂HP-β-CD	2.16×10^3	Tang *et al.*[47]
MSZ⊂P[5]Py	$(3.43 \pm 0.30) \times 10^3$	this work

MSZ: mesalazine; β-CD: β-cyclodextrin; HP-β-CD: hydroxypropyl-β-cyclodextrin; 18C6: 18-crown-6 ether.

Based on our previous studies[21] concerning the formation of inclusion complex between charged pillar[5] arenes and with aromatic guests, we have performed NOESY NMR experiments. Partial spectra (Figure 6), however, showed cross-peaks related to interactions between hydrogens from the pyridinium moieties with the aromatic ring hydrogen from mesalazine ascribed as a doublet of doublets at 6.69 ppm. This result corroborates with a supramolecular association whereas the MSZ molecules are accommodated in the entrance portals of the P[5]Py instead of inside the hydrophobic cavity (full NOESY spectra are shown in SI section, Figures S23-S25). No significant changes were observed in the FTIR of the complex (SI section, Figure S18).
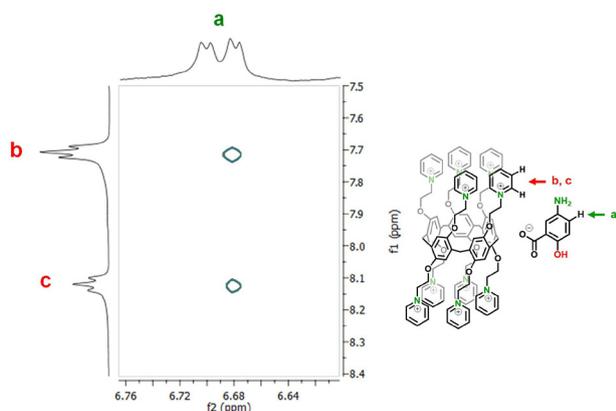

Figure 6. NOESY {1H-1H}NMR spectra for the P[5]Py:MSZ (both 1.4×10^{-4} mol L^{-1}) supramolecule in D$_2$O at pD = 7.9, evidencing the interactions between hydrogens of both compounds.

Dual static and dynamic quenching of fluorescence of 2,4,6-trinitrotoluene (TNT) explosive compound by pyridinium bromide decorated polymer was recently described, suggesting that pyridiniums played an important role in interacting with both ground and excited state.[48] Their studies resulted in the creation of an efficient probe for sensing explosive compounds in water. Our findings discussed above show a clear interaction between the compounds and we have also investigated the influence of pH on the quenching using an equimolar mixture of MSZ

and P[5]Py (Figure 7). Although the same profile was observed for pure MSZ solution, it is possible to observe that quenching of fluorescence takes place even under lower pH at a lower extent.
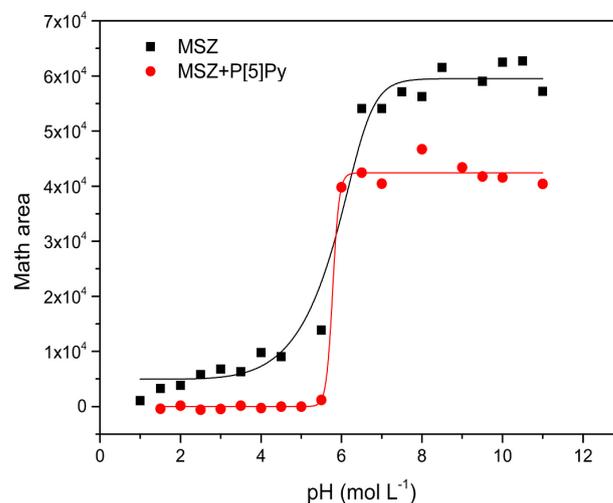

Figure 7. Quenching on fluorescence emission of MSZ (1.4×10^{-4} mol L^{-1}) in the presence of P[5]Py (1.4×10^{-4} mol L^{-1}) as a function of pH.

We have performed a Stern-Volmer quenching of fluorescence experiment. When the relationship between I_0 and I is evaluated as a function of the P[5]Py quencher concentration (Figure 8) whereas non-linear dependence on the intensity of fluorescence is observed, with an increase of quencher amount indicating that either dynamic or static quenching process may occur, not both.[49] Lifetime measurements were then determined leading to non-variable values (τ_0/τ, where $\tau_0 = 3.91$ ns) with the addition of P[5]Py, thus indicating that only static quenching occurs.[50] Also, the K_{SV} constant could be determined, by fitting data with equation 3, where I_0 and I are the fluorescence intensity of MSZ in the absence and presence of P[5]Py, respectively,
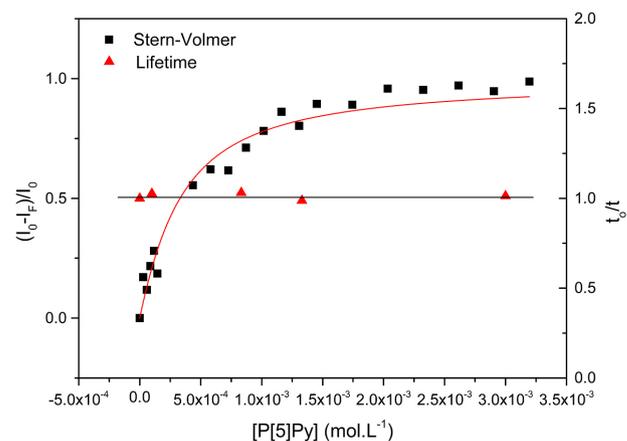

Figure 8. Stern-Volmer plot (black) and MSZ fluorescence lifetime τ_0/τ (red) measurements with increasing concentrations of P[5]Py quencher in aqueous medium at pH 7.5.

$[F_0]$ is the concentration of MSZ, $[Q_0]$ is the concentration of P[5]Py. The K_{SV} resulted in 3.99×10^3 mol L^{-1}, which represents a great interaction between MSZ and P[5]Py, and agrees with the values achieved from data depicted in Table 2 (more details available on SI section, Figures S20-S21).

$$\frac{I_0 - I}{I_0} = \frac{1}{2[F_0]}\left[\frac{1}{K_{SV}} + [F_0] + [Q_0] - \sqrt{\left(\frac{1}{K_{SV}} + [F_0] + [Q_0]\right)^2 - 4[F_0][Q_0]}\right] \quad (3)$$

Similar profiles of non-linear Stern-Volmer were also observed in a protein-fluorophore association related to different populations of interacting residues where only one is accessible to the quencher.[51] These are also related to the formation of aggregates in solution which deviates from the classical linear Stern-Volmer plot for static quenching of fluorescence.[52] With these data in hands we investigated a possible formation of aggregates between the molecules of P[5]Py which may cause even the observed shielding effect on the methylene bridged hydrogens observed in the ^{1}H NMR. Formation of polymer microfibers from a selftemplate assisted mechanism was recently described

for tosyl-pillarar[5]ene 6.[7] Although the authors did not mention it, the effect on the chemical shift was also prominent and these hydrogens resonate at 3.61 ppm. Conductimetric essay increasing the concentration of P[5]Py at pH 7.5 indeed showed a deviation from the curve for concentration around 1.0×10^{-5} mol L^{-1}, suggesting the formation of aggregates (see SI section, Figure S27). These aggregates are of high extension and the spheric model was used in DLS, resulting in particles around 400 nm (see SI section, Figure S26). Further experiments are being conducted which may increase the application of these compounds besides inclusion complex formation.

Theoretical calculations

The MSZ and P[5]Py systems were calculated using Orca quantum package. The molecules were fully optimized using DFT/bp86 calculations (optimized coordinates are available on Tables S1-S3, SI section). The MSZ molecule was calculated assuming their form at pH 7 and, as observed (Figure 9a), possesses a linear arrangement where a negative charge is localized on O atoms of the
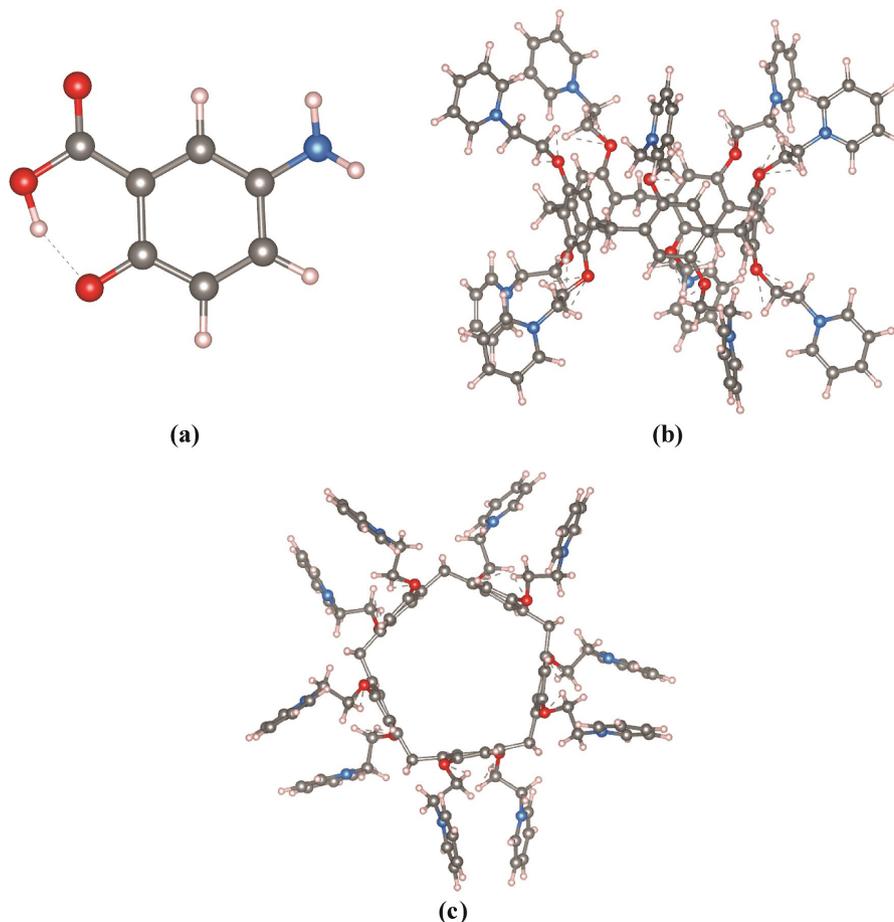

(a)   **(b)**

(c)

Figure 9. Fully-optimized structures obtained from DFT calculations. (a) MSZ, (b) side-view of P[5]Py, and (c) top-view of P[5]Py. The C, H, O, and N atoms are represented in gray, light pink, red, and cyan colors, respectively.

carboxylic acid functional group, as expected. In the case of P[5]Py, the calculated conformation indicates a pilar structure with opened portals (Figure 9b) and a hydrophobic cavity within aromatic rings forming a cyclopentane-like form (Figure 9c). This macromolecule presents ten positive charges on pyridine N atoms that interact with Br or OTs ions; the calculations carried out in this work evaluate the charged form of P[5]Py without counter ions. Once the structural analysis was performed, the next step lies in assessing the excited states for P[5]Py and MSZ systems from TDDFT calculations. The results enable us to predict the UV-Vis for both molecules in the water solvent media. For MSZ (Figure S28, SI section), an absorption band was found at 338 nm agreeing with experimental analysis performed in this work assuming a pH of 7 (Figure 3). The TDDFT indicates that such absorption refers to the LUMO←HOMO electronic transitions (Figure 10) and the energy involved in such transition is 3.67 eV.

Finally, after evaluating MSZ and P[5]Py system in isolated form, quantum simulations were performed to
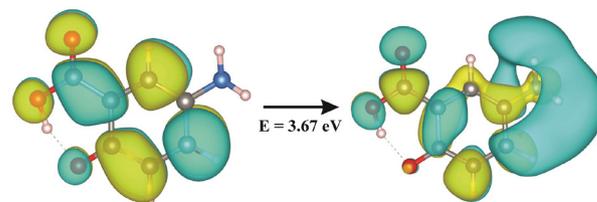

Figure 10. Molecular orbitals involved in UV-Vis transitions for MSZ. The C, H, O, and N atoms are represented in gray, light pink, red, and cyan colors, respectively.

predict the interaction between P[5]Py and MSZ molecules. The fully optimized model indicates that the interaction occurs between C atoms from the pyridine groups from P[5]Py and O from carboxylate on MSZ, as demonstrated in Figure 11. Therefore, the results suggest that both molecules interact through electrostatic interaction since each MSZ molecule can replace a Br or OTs counter ion. The obtained system agrees with the NOESY {^{1}H^{1}H}NMR spectra (Figure 6) because of the proximity between H atoms from MSZ and pyridine.
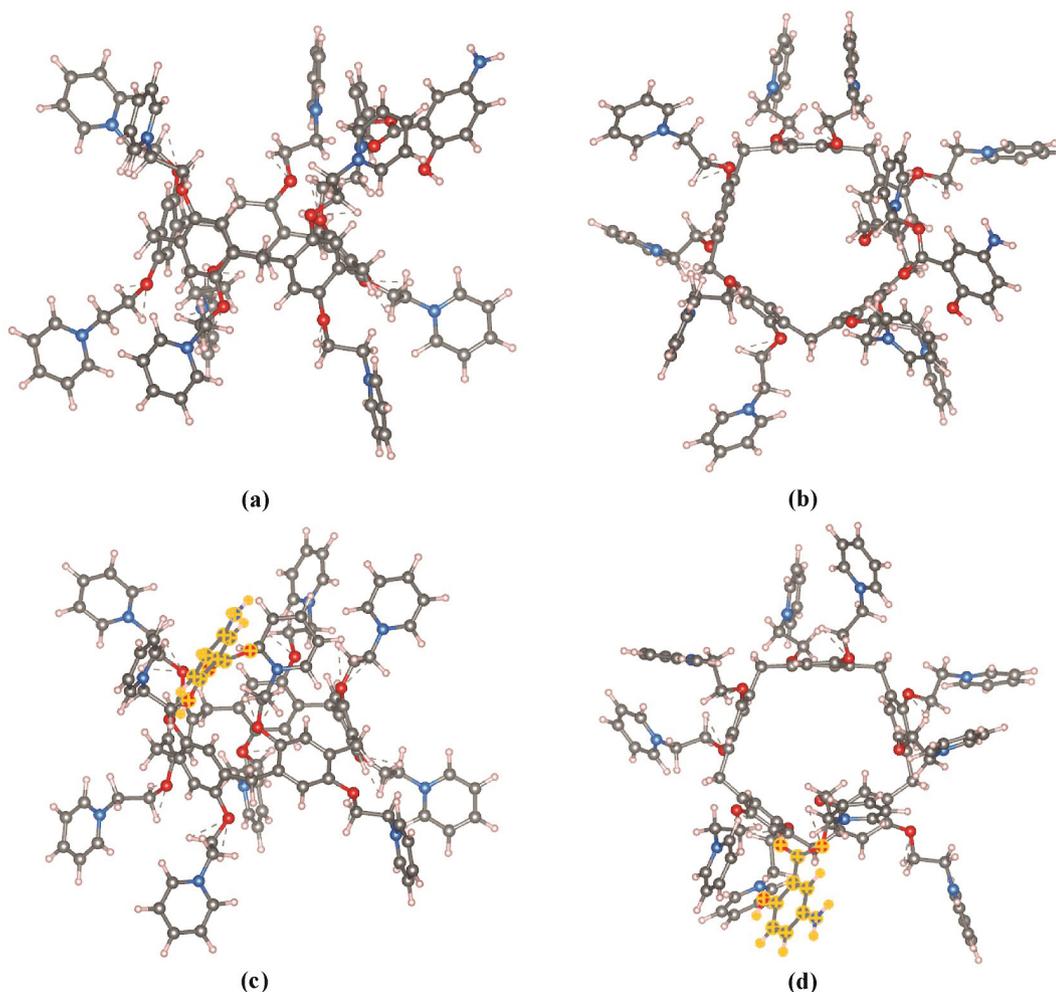

Figure 11. MSZ and P[5]Py interaction. (a) Side view; (b) top view; (c) side view and (d) top view with MSZ molecule highlighted. The C, H, O, and N atoms are represented in gray, light pink, red, and cyan colors, respectively.

J. Braz. Chem. Soc. **2024**, *35*, 1, e-20230106

9 of 11

Conclusions

In this work, we have synthesized a cationic pyridinium-pillar[5]arene from previously prepared pertosylated pillar[5]arene and we investigated the formation of supramolecular mesalazine pillar[5]arene complexes. Initially, the pK_a values of mesalazine were determined and the spectroscopic properties of the molecule as a function of pH were evaluated. The highest intensity of fluorescence emission was observed under physiological conditions, where the anionic form of mesalazine is present. Although a classical inclusion complex was not observed from host-guest interactions at pH 7.5, interaction between both compounds causes drastic changes in spectroscopic properties of mesalazine. Static quenching of fluorescence was observed in physiological conditions and no changes in fluorescence lifetimes were observed when increasing the concentration of the macrocycle. The theoretical results indicate that the interaction between pyridinium-pillar[5]arene macrocycle and mesalazine drug occurs due to strong electrostatic attraction. More precisely, the O atoms from the carboxylate of mesalazine interact with a C atom from pyridine replacing a counter ion. The quenching fluorescence with complexation can be used as a strategy for the detection of mesalazine, under physiological conditions, by fluorescence spectroscopy. In addition, the great association of mesalazine and pillar[5]arene is an important factor for development of pillar[5]arene-based delivery systems.

Supplementary Information

Supplementary information (Figures S1 to S28 and Table S1 to S3) is available free of charge at http://jbcs.sbq.org.br as PDF file.

Acknowledgments

Author Contributions

Willian Demos was responsible for conceptualization, investigation, visualization and writing original draft; Lizandra C. B. Micke for investigation and methodology; Luis H. S. Lacerda for formal analysis; Bruno S. de Souza for conceptualization and methodology; Adriana P. Gerola for conceptualization, methodology and writing review and editing; Ricardo F. Affeldt for supervision, conceptualization, writing original draft.

References

1. Ogoshi, T.; Kanai, S.; Fujinami, S.; Yamagishi, T.; Nakamoto, Y.; *J. Am. Chem. Soc.* **2008**, *130*, 5022. [Crossref]

2. Chen, J.-F.; Lin, Q.; Zhang, Y.-M.; Yao, H.; Wei, T.-B.; *Chem. Commun.* **2017**, *53*, 13296. [Crossref]

3. Li, Y.; Wen, J.; Li, J.; Wu, Z.; Li, W.; Yang, K.; *ACS Sens.* **2021**, *6*, 3882. [Crossref]

4. Zhou, Y.; Jie, K.; Huang, F.; *Org. Chem. Front.* **2017**, *4*, 2387. [Crossref]

5. Ogoshi, T.; Yamagishi, T.; *Eur. J. Org. Chem.* **2013**, *2013*, 2961. [Crossref]

6. Al-Azemi, T. F.; Vinodh, M.; Alipour, F. H.; Mohamod, A. A.; *RSC Adv.* **2019**, *9*, 13814. [Crossref]

7. Ruengsuk, A.; Khamphaijun, K.; Pananusorn, P.; Docker, A.; Tantirungrotechai, J.; Sukwattanasinitt, M.; Harding, D. J.; Bunchuay, T.; *Chem. Commun.* **2020**, *56*, 8739. [Crossref]

8. Silveira, E. V.; Nascimento, V.; Wanderlind, E. H.; Affeldt, R. F.; Micke, G. A.; Garcia-Rio, L.; Nome, F.; *J. Org. Chem.* **2019**, *84*, 9684. [Crossref]

9. Fernando, A.; Mako, T. L.; Levenson, A. M.; Cesana, P. T.; Mendieta, A. M.; Racicot, J. M.; DeBoef, B.; Levine, M.; *Supramol. Chem.* **2019**, *31*, 545. [Crossref]

10. Lan, S.; Zhan, S.; Ding, J.; Ma, J.; Ma, D.; *J. Mater. Chem. A* **2017**, *5*, 2514. [Crossref]

11. Santos, E. C. S.; dos Santos, T. C.; Fernandes, T. S.; Jorge, F. L.; Nascimento, V.; Madriaga, V. G. C.; Cordeiro, P. S.; Checca, N. R.; Costa, N. M. D.; Pinto, L. F. R.; Ronconi, C. M.; *J. Mater. Chem. B* **2020**, *8*, 703. [Crossref]

12. Nazarova, A. A.; Yakimova, L. S.; Padnya, P. L.; Evtugyn, V. G.; Osin, Y. N.; Cragg, P. J.; Stoikov, I. I.; *New J. Chem.* **2019**, *43*, 14450. [Crossref]

13. Yue, L.; Yang, K.; Lou, X.-Y.; Yang, Y.-W.; Wang, R.; *Matter* **2020**, *3*, 1557. [Crossref]

14. Zhu, H.; Liu, J.; Shi, B.; Wang, H.; Mao, Z.; Shan, T.; Huang, F.; *Mater. Chem. Front.* **2018**, *2*, 1475. [Crossref]

15. Yang, Q.; Xu, W.; Cheng, M.; Zhang, S.; Kovaleva, E. G.; Liang, F.; Tian, D.; Liu, J.; Abdelhameed, R. M.; Cheng, J.; Li, H.; *Chem. Commun.* **2022**, *58*, 3255. [Crossref]

16. Diez, N. M.; de la Peña, A. M.; García, M. C. M.; Gil, D. B.; Cañada-Cañada, F.; *J. Fluoresc.* **2007**, *17*, 309. [Crossref]

17. Elbashir, A. A.; Dsugi, N. F. A.; Aboul-Enein, H. Y.; *J. Fluoresc.* **2014**, *24*, 355. [Crossref]

18. Chao, J.-B.; Tong, H.-B.; Huang, S.-P.; Liu, D.-S.; *Spectrochim. Acta, Part A* **2004**, *60*, 161. [Crossref]

19. Linares, M.; De Bertorello, M. M.; Longhi, M.; *Molecules* **2000**, *5*, 342. [Crossref]

20. Silveira, E. V.; Wanderlind, E. H.; Masson, A. K.; Cordeiro, P. S.; Nascimento, V.; Affeldt, R. F.; Micke, G. A.; *New J. Chem.* **2020**, *44*, 2701. [Crossref]

21. Giusti, L. A.; Medeiros, M.; Ferreira, N. L.; Mora, J. R.; Fiedler, H. D.; *J. Phys. Org. Chem.* **2014**, *27*, 297. [Crossref]

22. Silveira, E. V.; Montecinos, R.; Scorsin, L.; Garcia-Rio, L.; Medeiros, M.; Nascimento, V.; Nome, F.; Affeldt, R. F.; Micke, G. A.; *New J. Chem.* **2021**, *45*, 6486. [Crossref]

23. Joseph, R.; Naugolny, A.; Feldman, M.; Herzog, I. M.; Fridman, M.; Cohen, Y.; *J. Am. Chem. Soc.* **2016**, *138*, 754. [Crossref]

24. Kaizerman-Kane, D.; Hadar, M.; Joseph, R.; Logviniuk, D.; Zafrani, Y.; Fridman, M.; Cohen, Y.; *ACS Infect. Dis.* **2021**, *7*, 579. [Crossref]

25. Song, N.; Lou, X.-Y.; Ma, L.; Gao, H.; Yang, Y.-W.; *Theranostics* **2019**, *9*, 3075. [Crossref]

26. Ng, S. C.; Shi, H. Y.; Hamidi, N.; Underwood, F. E.; Tang, W.; Benchimol, E. I.; Panaccione, R.; Ghosh, S.; Wu, J. C. Y.; Chan, F. K. L.; Sung, J. J. Y.; Kaplan, G. G.; *Lancet* **2017**, *390*, 2769. [Crossref]

27. Alatab, S.; Sepanlou, S. G.; Ikuta, K.; Vahedi, H.; Bisignano, C.; Safiri, S.; Sadeghi, A.; Nixon, M. R.; Abdoli, A.; Abolhassani, H.; Alipour, V.; Almadi, M. A. H.; Almasi-Hashiani, A.; Anushiravani, A.; Arabloo, J.; Atique, S.; Awasthi, A.; Badawi, A.; Baig, A. A. A.; Bhala, N.; Bijani, A.; Biondi, A.; Borzì, A. M.; Burke, K. E.; Carvalho, F.; Daryani, A.; Dubey, M.; Eftekhari, A.; Fernandes, E.; Fernandes, J. C.; Fischer, F.; Haj-Mirzaian, A.; Haj-Mirzaian, A.; Hasanzadeh, A.; Hashemian, M.; Hay, S. I.; Hoang, C. L.; Househ, M.; Ilesanmi, O. S.; Jafari Balalami, N.; James, S. L.; Kengne, A. P.; Malekzadeh, M. M.; Merat, S.; Meretoja, T. J.; Mestrovic, T.; Mirrakhimov, E. M.; Mirzaei, H.; Mohammad, K. A.; Mokdad, A. H.; Monasta, L.; Negoi, I.; Nguyen, T. H.; Nguyen, C. T.; Pourshams, A.; Poustchi, H.; Rabiee, M.; Rabiee, N.; Ramezanzadeh, K.; Rawaf, D. L.; Rawaf, S.; Rezaei, N.; Robinson, S. R.; Ronfani, L.; Saxena, S.; Sepehrimanesh, M.; Shaikh, M. A.; Sharafi, Z.; Sharif, M.; Siabani, S.; Sima, A. R.; Singh, J. A.; Soheili, A.; Sotoudehmanesh, R.; Suleria, H. A. R.; Tesfay, B. E.; Tran, B.; Tsoi, D.; Vacante, M.; Wondmieneh, A. B.; Zarghi, A.; Zhang, Z.-J.; Dirac, M.; Malekzadeh, R.; Naghavi, M.; *Lancet Gastroenterol. Hepatol.* **2020**, *5*, 17. [Crossref]

28. Homepage | Crohn's & Colitis Foundation, https://www.crohnscolitisfoundation.org/, accessed in June 2023.

29. Elbashir, A. A.; Abdalla, F. A. A.; Aboul-Enein, H. Y.; *Luminescence* **2015**, *30*, 1250. [Crossref]

30. Elbashir, A. A.; Abdalla, F. A. A.; Aboul-Enein, H.; *Luminescence* **2015**, *30*, 444. [Crossref]

31. Morcoss, M. M.; Abdelwahab, N. S.; Ali, N. W.; Elsaady, M. T.; *Chem. Pharm. Bull.* **2016**, *64*, 1268. [Crossref]

32. *Origin*, version 8,0; OriginLab Corporation, Northampton, MA, USA.

33. Pozdnyakov, I. P.; Pigliucci, A.; Tkachenko, N.; Plyusnin, V. F.; Vauthey, E.; Lemmetyinen, H.; *J. Phys. Org. Chem.* **2009**, *22*, 449. [Crossref]

34. Xue, M.; Yang, Y.; Chi, X.; Zhang, Z.; Huang, F.; *Acc. Chem. Res.* **2012**, *45*, 1294. [Crossref]

35. Bannwarth, C.; Ehlert, S.; Grimme, S.; *J. Chem. Theory Comput.* **2019**, *15*, 1652. [Crossref]

36. Grimme, S.; Bannwarth, C.; Shushkov, P.; *J. Chem. Theory Comput.* **2017**, *13*, 1989. [Crossref]

37. Kohn, W.; Sham, L. J.; *Phys. Rev.* **1965**, *140*, A1133. [Crossref]

38. Grimme, S.; Antony, J.; Ehrlich, S.; Krieg, H.; *J. Chem. Phys.* **2010**, *132*, 154104. [Crossref]

39. Neese, F.; Wennmohs, F.; Becker, U.; Riplinger, C.; *J. Chem. Phys.* **2020**, *152*, 224108. [Crossref]

40. Abdolmohammad-Zadeh, H.; Kohansal, S.; *J. Braz. Chem. Soc.* **2012**, *23*, 473. [Crossref]

41. Abdalla, F.; Elbashir, A.; *J. Med. Chem.* **2014**, *4*, 361. [Crossref]

42. Gutz, I. G. R.; *CurTiPot-pH and Acid-Base Titration Curves: Analysis and Simulation freeware*, version 4.3.1; Universidade de São Paulo, 2021.

43. Sobolewski, A. L.; Domcke, W.; *Chem. Phys.* **1998**, *232*, 257. [Crossref]

44. Maheshwari, S.; Chowdhury, A.; Sathyamurthy, N.; Mishra, H.; Tripathi, H. B.; Panda, M.; Chandrasekhar, J.; *J. Phys. Chem. A* **1999**, *103*, 6257. [Crossref]

45. Joshi, H. C.; Antonov, L.; *Molecules* **2021**, *26*, 1475. [Crossref]

46. Karpour, M.; Alizadeh, N.; *Polym. Bull.* **2023**, *80*, 3021. [Crossref]

47. Tang, P.; Sun, Q.; Zhao, L.; Pu, H.; Yang, H.; Zhang, S.; Gan, R.; Gan, N.; Li, H.; *Carbohydr. Polym.* **2018**, *198*, 418. [Crossref]

48. Tanwar, A. S.; Parui, R.; Garai, R.; Chanu, M. A.; Iyer, P. K.; *ACS Meas. Au* **2022**, *2*, 23. [Crossref]

49. Gehlen, M. H.; *J. Photochem. Photobiol., C* **2020**, *42*, 100338. [Crossref]

50. Ciotta, E.; Prosposito, P.; Pizzoferrato, R.; *J. Luminescence* **2019**, *206*, 518. [Crossref]

51. Nasri, R.; Bidel, L. P. R.; Rugani, N.; Perrier, V.; Carrière, F.; Dubreucq, E.; Jay-Allemand, C.; *Molecules* **2019**, *24*, 2888. [Crossref]

52. Hwang, Y. L.; Hwang, K. C.; *Fullerene Sci. Technol.* **1999**, *7*, 437. [Crossref]

J. Braz. Chem. Soc. **2024**, *35*, 1, e-20230106

11 of 11